Rayleigh and shear-horizontal surface acoustic waves simultaneously generated in inclined ZnO films for acoustofluidic lab-on-a-chip

Hua-Feng Pang, [1,2] Ran Tao,[3,2] Jingting Luo,[3,2] Xiaosong Zhou,[4] Jian Zhou,[5] Glen McHale,[6] Julien Reboud,[7] Hamdi Torun,[2] D. Gibson,[8] KaiTao,[9] Honglong Chang,[9] Yong-Qing Fu,[2*]

1. Department of Applied Physics, College of Science, Xi'an University of Science and Technology, Xi'an, 710054, P. R. China

2. Faculty of Engineering and Environment, Northumbria University, Newcastle upon Tyne, NE1 8ST, UK.

3. Key Laboratory of Optoelectronic Devices and Systems of Education Ministry and Guangdong Province, College of Physics and Optoelectronic Engineering, Shenzhen University, Shenzhen 518060, P. R. China

4. Institute of Nuclear Physics and Chemistry, China Academy of Engineering Physics, Mianyang, 621900, P. R. China

5. College of Mechanical and Vehicle Engineering, Hunan University, Changsha 410082, P. R. China

6. Institute for Multiscale Thermofluids, School of Engineering, University of Edinburgh, Edinburgh, EH9 3FB, UK.

7. Division of Biomedical Engineering, James Watt School of Engineering, University of Glasgow, GlasgowG12 8LT, UK.

8. Institute of Thin Films, Sensors & Imaging, University of the West of Scotland, Scottish Universities Physics Alliance, Paisley PA1 2BE, UK.

[*]corresponding author, Prof. Richard Yongqing Fu, E-mail: richard.fu@northumbria.ac.uk

9. Key Laboratory of Micro and Nano Systems for Aerospace, Ministry of Education, Northwestern Polytechnical University, Xi'an 710072, P. R. China.

Abstract

There are significant challenges in controlling uniformity of crystal inclination angles, growth orientations and film thicknesses to generate dual-mode surface acoustic waves (e.g., Rayleigh ones and shear-horizontal ones) for lab-on-a-chip applications. In this study, we demonstrate large area (up to three inches) and uniformly inclined piezoelectric ZnO films, sputtering-deposited on silicon using a glancing angle deposition method. Characterization using X-ray diffraction showed that the inclined ZnO films have an average crystal inclination angle of 29.0°, apart from the vertical (0002) orientation, at a substrate tilting angle of 30°. Reflection signals of ZnO/Si surface acoustic wave devices clearly show the generations of both shear horizontal surface acoustic waves and Rayleigh waves. The Rayleigh waves enable efficient acoustofluidic functions including streaming and transportation of sessile droplets. Excitation direction of Rayleigh waves on the acoustofluidics versus the inclined angle direction has apparent influences on the acoustofluidic performance due to the anisotropic microstructures of the inclined films. The same device has been used to demonstrate biosensing of biotin/streptavidin interactions in a liquid environment using the shear-horizontal surface acoustic waves, to demonstrate its potential for integration into a complete lab-on-a-chip device.

Keywords: ZnO film, *c*-axis inclined orientation, shear horizontal-SAW, acoustofluidics

1. **Introduction**

Surface acoustic waves (SAWs) have attracted extensive interest in biosensing, microfluidics, quantum acoustics, and lab-on-a-chip (LOC) applications [1-4], with their abilities to generate all the required functions (e.g., sensing, liquid mixing, transportation, jetting and nebulization) on a single LOC [5-8]. However, each functionality is often enabled by a certain acoustic mode, which generally requires different geometries and devices, making it a great challenge to integrate all aspects onto a single LOC. Among the different modes of SAWs, Rayleigh mode SAWs are generated by patterning interdigital transducers (IDTs) on piezoelectric bulk materials such as 128° Y-cut $LiNbO_3$, or *c*-axis (or vertically) textured thin films such as zinc oxide (ZnO), aluminum nitride (AlN), and gallium nitride [9-12]. They have been applied in gas sensing, ultraviolet light sensing, biosensing, and acoustofluidics [13-14]. The Rayleigh SAWs can actuate liquid in a droplet format or within a microchannel to realize acoustofluidics due to the strong coupling of the dissipated wave energy into the liquid [15]. However, significant energy dissipation also leads to limitations for most biosensing functions in a liquid environment due to the damping of the SAW signals. In contrast, there is minimal damping or attenuation of shear-horizontal surface acoustic waves (SH-SAWs) into the liquid, because the SH-SAWs are acoustic waves that propagate in plane on the substrate and their displacements are parallel to the substrate surface [16]. SAW biosensors based on the SH-SAWs have been shown to achieve excellent sensitivities in the liquid environment [17-19]. Therefore, a single SAW device, which can simultaneously generate the above two modes, has the potential to enable both functions (i.e., sensing and bio-sampling) in a single LOC system.

The orientation of piezoelectric thin films critically determines the acoustic wave modes and performance of thin film-based acoustic devices [20]. For example, SH-SAWs can be generated in AlN film SAWs with a *c*-axis film inclination of ~10° [21]. ZnO based ultrasonic transducers with a *c*-axis tilted angle of ~25° or c-axis zigzag ZnO films can generate both longitudinal and shear waves [22, 23].

Shear mode film bulk wave resonator (FBAR) based on inclined *c*-axis ZnO films with an inclined angle of ~25° achieved a mass sensitivity of 4.9±0.1 kHz·cm^2·ng^{-1} [24]. Pure longitudinal and shear modes have been excited in ZnO FBARs with the *c*-axis tilted angles of 15° and 30° [25].

Theoretical analysis indicated that the maximum value of the electromechanical coefficient for the bulk shear waves was obtained at a crystal inclination angle of 28° in the *c*-axis inclined bulk ZnO [26]. For *c*-axis inclined bulk AlN, the corresponding maximum value is at a *c*-axis inclined angle of 50° [27], whilst it was predicted at an inclined angle of 33° in the c-axis tilted ScAlN films [28]. Experimentally, Rayleigh SAWs are excited on the devices fabricated using vertical ZnO films [6,11,15], whilst SH-SAW are generated on the devices made of $(11\bar{2}0)$ ZnO films, *c*-axis inclined AlN and Sc doped AlN film [20,29,30].

To date, SH-SAWs and Rayleigh waves are difficult to be simultaneously generated in the *c*-axis inclined film-based SAW devices [21,31]. For example, in our previous study of ultrasonic transducers [32], we have grown the *c*-axis inclined ZnO films by tilting the substrate during deposition, and successfully achieved both the longitudinal and shear bulk waves. However, using the same inclined ZnO films, we could not simultaneously generate both the SH-SAWs and Rayleigh waves in a single SAW device. In literature, there are few papers which have reported the successful generation and application of the dual mode SAW devices. As explained clearly in our recent review paper [33], the main difficulties are the precise control of (a) the inclination of wurtzite crystal orientations (not the columnar orientation which is easily obtained and commonly reported), and (b) the uniformity of the inclined ZnO film thickness and crystallinity, as well as (c) surface roughness over a large area (e.g., across a whole wafer to enable integration into microfabrication foundries). Furthermore, the porous and columnar structures that are associated with the highly inclined ZnO films often result in very weak SH-SAW signals [31,33].

Magnetron sputtering has been commonly used for preparing the inclined ZnO films based on the glancing angle deposition (GLAD) method, which can be applied to tailor the crystal orientations of ZnO films along both out-of-plane and in-plane directions [21-25]. The quality of the inclined ZnO films is dependent on the deposition conditions such as substrate-tilting angle, deposition rate, chamber pressure, Ar/O_2 gas ratio, and bias voltage [34-36].

In this paper, to simultaneously generate both SH-SAWs and Rayleigh waves, we optimized the process parameters to deposit *c*-axis inclined ZnO films using the GLAD method, by selecting an optimized Ar/O_2 gas ratio and a suitable chamber pressure. The *c*-axis inclined crystal structures were systematically analyzed and dual mode SAWs were successfully generated on the inclined ZnO films. Using the dual mode SAW devices, integrated functions of acoustofluidics and biosensing were demonstrated.

2. **Experimental details**

ZnO films were deposited on silicon (100) substrates using a direct current magnetron sputtering equipment (Nordiko Technical Services Ltd.) and a Zn target (with a size of 10×30 cm^2 and a purity of 99.99%). The silicon substrates were loaded into the chamber and fixed onto a holder facing the sputtering target at oblique angles of 0° (standard deposition position) and 30°during the deposition. The base pressure in the chamber was 2.2×10^{-3} Pa, which was obtained using a pumping system including a turbomolecular pump (Balzers IMG 060B) and a mechanical pump (Edwards EH1200). The optimized chamber pressure was 0.11Pa, controlled using a Balzers Pirani gauge. Argon and oxygen gases with their corresponding flow rates of 10 sccm and 12 sccm were introduced into the chamber, and their flow rates were controlled using flow controllers (Multi-gas Controller 647B, MKS instruments Co.). During

the deposition, the applied DC power was 450 W. The deposition rate was ~0.8 μm per hour on the substrates without a tilted angle and ~0.6 μm per hour on the substrates with a tilted angle of 30°.

Surface morphology and cross-sectional microstructures were characterized using a scanning electron microscope (SEM, MIRA3, TESCAN). Surface roughness of the films was measured in an area of 10×10 μm^2 at three different positions of the sample surface using an atomic force microscope (AFM, CSPM4000, Ben-Yuan). Structural analysis and crystalline orientation of the ZnO films were characterized using X-ray diffraction (XRD, D8 Discover A25, Bruker) with Cu Kα radiation (λ = 1.5406Å). Film texture was analyzed based on the Bragg Brentano XRD measurement with a θ-2θ scanning method, and the pole figures were obtained using the XRD patterns that were measured by rotating the sample for 360° with a 5° interval.

SAW devices were fabricated using the conventional photolithography and lift-off processes. Bilayers of the Cr/Au films (20nm/100nm) were deposited as the electrodes on the surface of ZnO films using an electron beam evaporator. The obtained devices have two ports of the IDTs that were composed of 60 pairs of fingers and a spatial periodicity of 64 μm. The reflection signals (S_{11}) of the ZnO SAW devices were measured using a radio frequency (RF) network analyzer (HP8752A, Keysight). The ZnO SAW device was heated from 50 ℃ to160 ℃ in an environment-controlled chamber to determine its temperature coefficient of the frequency (*TCF*), using a formula of $TCF = -\Delta f / (\Delta T \times f)$, where f is the resonant of the SAW device, Δf and ΔT are the variations of the frequency shift and temperature change, respectively.

For microfluidic tests, the IDTs of the SAW devices were connected to a power amplifier (Amplifier Research, 75A250, Souderton, USA), and the input signal was generated from an RF signal generator (Marconi 2024, Plainview, USA). The device's surface including the IDTs was treated with 1% CYTOP solution (L-809A) by drop-coating, followed by heating at 120 ℃ for ~5 minute to form a hydrophobic

surface. The static contact angles were measured as ~110^{o}. Droplet movement after the excitation of the RF signal to the IDTs was recorded using a standard CMOS camera.

For biosensing tests, the IDTs of the SAW devices were pre-coated with an insulating layer of SiO_2 (50 nm thick). A polydimethylsiloxanes (PDMS) chamber (0.5×0.5×0.5 cm^3) was fabricated and bonded onto the pre-coated IDTs using oxygen plasma. The inner chamber was cleaned using ethanol and de-ionized water for three times. Then the chamber was incubated with ~40 μL of the biotin solution for one hour, followed by rinsing with phosphate buffered saline (PBS, 10 mM phosphate, 150 mM NaCl, pH=7.4). Streptavidin conjugated silica microspheres (in a diameter of 5μm) were suspended in the PBS buffer solutions with different concentrations and added into the chamber. The interaction of the streptavidin with the biotin was monitored by tracking the resonant frequency of SH-SAWs based on the reflection spectra (S_{11}), which were recorded from the network analyzer. The chamber was cleaned using the PBS buffer solution before each test with the different streptavidin concentrations. The biotin and streptavidin conjugated silica microspheres were purchased from Sigma-Aldrich Company.

3. **Results and discussion**

3.1 Microstructures and texture analysis

Figure 1 shows cross-sectional SEM images of the ZnO films on silicon. When the substrate tilting angles were changed from 0° to 30°, the microstructure in the ZnO films was changed from vertical columns to inclined columns. Cross-sectional microstructure of the ZnO films deposited at the substrate tilting angle of 30° (see Figure 2b) clearly shows that the inclined columns appear to have two different features. In the initial stage of growth, microstructures show both the vertical columns and inclined columns up to film

thickness of 1~2 μm from the substrate surface. The growth of inclined columns is subsequently dominant for the thickness lager than ~2 μm and the columnar inclination angle was roughly estimated as 27°±3°.

Figures 1c-1d show the surface morphologies of the ZnO films. The average aspect ratio (e.g., the ratio between its length to width) for the surface features of column tops are measured to be 1.8±0.6 and 2.8±0.9 for the ZnO films deposited at the substrate tilting angle of 0° and 30°, respectively. The shape of the column tops is significantly elongated along the direction of the incident flux at the substrate tilting angle of 30°. The morphological change of the film with the substrate tilting angle of 30° is due to the in-plane growth rate anisotropy formed by the biased diffusion of the arriving species with the in-plane momentum and the anisotropy of the capture length for diffusing particles [37,38]. Considering the difference of the in-plane growth rate anisotropy for the tilted and non-titled films, the incoming species arrived on the surface of the tilted sample have a larger momentum in-plane that could diffuse a longer distance, which contributes the elongated granular morphology on the surface of the tilted sample [38-40].

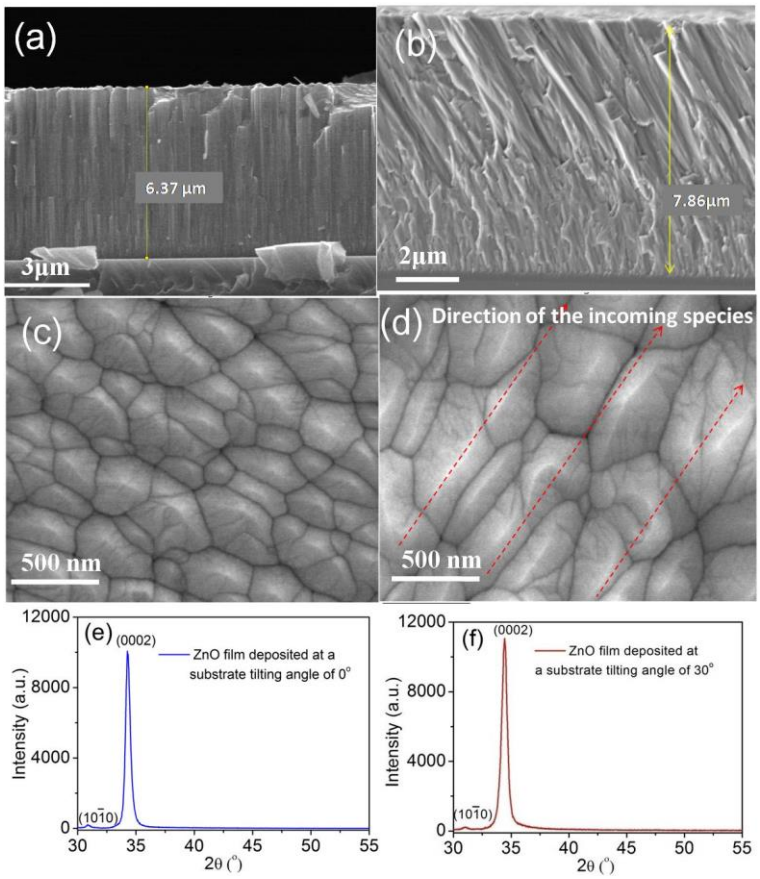

Figure 1. Cross-section and surface morphologies of the ZnO films deposited with different substrate tilting angles: (a, c) 0°; (b, d) 30° (the dotted lines in the (d) show the inclined direction); XRD patterns of the ZnO films on silicon substrates deposited at different substrate tilting angles of (e) 0°; (f) 30°.

Figures 1e-1f present the XRD spectra of the ZnO films deposited on silicon substrates. The two peaks in the XRD patterns can be indexed to the wurtzite structure of ZnO. The strong (0002) diffraction peaks indicate that the preferential growth of the ZnO films is along the *c*-axis perpendicular to the film surface in the sputtering process. Although the analysis is only based on one peak, the observed shift of this peak from 34.26° to 34.44° with the substrate tilting angle changed from 0° to 30°suggests that there are compressive stresses in the films. The film stress is decreased with the inclination angle due to the existence of porous and nano-columnar microstructures. The crystallite (or domain) sizes of the ZnO films were estimated using the Debye-Scherrer formula and the calculated values are17±2 nm and 35±4 nm,

respectively [40]. In addition, the average root-mean-square roughness was obtained using the AFM and the data are 5.9±1.7 nm and 13.1±2.2 nm for these two films, respectively.

Pole-figure analysis was performed using the XRD to obtain the crystal inclination of texture structure. As expected, the ZnO film with the substrate tilting angle of 0° (standard deposition) has a strong pole figure of {0001}. Figures 2a-2e show the XRD pole figures obtained from the {0001}, $\{10\bar{1}0\}$, $\{10\bar{1}1\}$, $\{10\bar{1}2\}$, $\{10\bar{1}3\}$ and $\{12\bar{2}0\}$ reflections of the ZnO film with the substrate tilting angle of 30°. The localized {0001} pole is deviated from the central region, suggesting that the ZnO film has a *c*-axis crystal inclination angle of 29.0°±0.5° from the normal, which is generated under the continuous impingement of the incoming atoms with an incidence angle. The $\{10\bar{1}0\}$ pole is relatively weak and is asymmetrically distributed at the central region. All the other pole figures do not show strong localization. These results verify the formation of the ZnO crystalline structure with an inclined angle. Combining the results of the SEM and XRD analysis, we can conclude that there are mixed orientations of the c-axis inclined angled crystals (under the continuously impingement of the incoming atoms with an incidence angle) and vertical *c*-axis orientation (which are mainly formed at the initial stage) in the inclined columnar ZnO film.

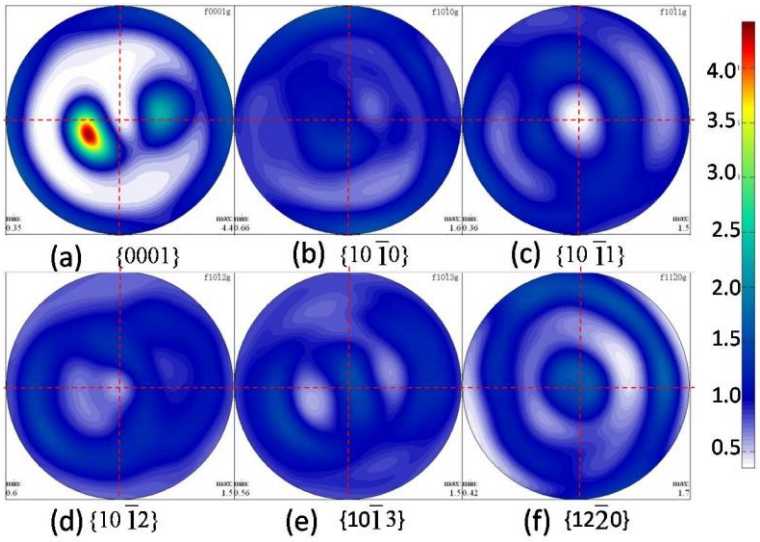

Figure 2.Pole figures of ZnO films from the different crystallographic diffractions of (a) {0001}, (b){$10\bar{1}$0}, (c){$10\bar{1}1$}, (d) {$10\bar{1}2$},(e){$10\bar{1}3$}, and (f){$12\bar{2}0$}.

3.2 Dual mode SAWs and excitation direction of Rayleigh SAWs

Reflection signals (S_{11}) of the ZnO SAW devices are shown in Figure 3a. Both the Rayleigh SAWs and SH-SAWs are successfully detected from the resonant characteristics of the inclined ZnO film-based SAW devices. The peaks of the Rayleigh SAWs are at 67.38 MHz, and 60.47 MHz, corresponding to the phase velocities of 4312.32 $m \cdot s^{-1}$and 3870.08 $m \cdot s^{-1}$ for the ZnO SAW devices with the substrate tilting angles of 0° and 30°, respectively. The peak of SH-SAW for the SAW device using the inclined ZnO film is at 89.93 MHz, corresponding to the phase velocity of 5755.52 $m \cdot s^{-1}$. The phase velocity of the SH-SAW at this film/substrate configuration is much larger than that of the Rayleigh mode SAW, which has been reported in the inclined AlN SAW devices, as well as the 36° Y-cut $LiTaO_3$ SAW device [41,42]. The Sezawa wave modes can also be detected, which exhibit spurious ripples in the region from 95 MHz to 120 MHz due to a strong triple transit effect [43]. The frequency of SH-SAW is close to that of the Sezawa wave, which might cause confusion for their identifications.

Figure 3b shows the frequency shifts of the Rayleigh waves varied with the ambient temperature for the ZnO SAW devices obtained from the two types of films. The temperature sensitivity becomes slightly less significant when the substrate tilting angle is changed from 0° to 30° based on the comparison of the frequency shifts between the two samples. The variation of the TCF values from −37.1 $ppm \cdot ℃^{-1}$ to −33.9 $ppm \cdot ℃^{-1}$ indicates that the temperature stability has been slightly improved using the inclined ZnO films. The thermal expansion coefficient of the ZnO film could have been decreased due to the lower elastic moduli of inclined angled films and relatively difficult thermal diffusion among the nanoscale columnar structures [44]. Therefore, the frequency shifts induced by the expansion and deformation of the inclined films become less prominent than those of the ZnO film with vertical crystal inclination.

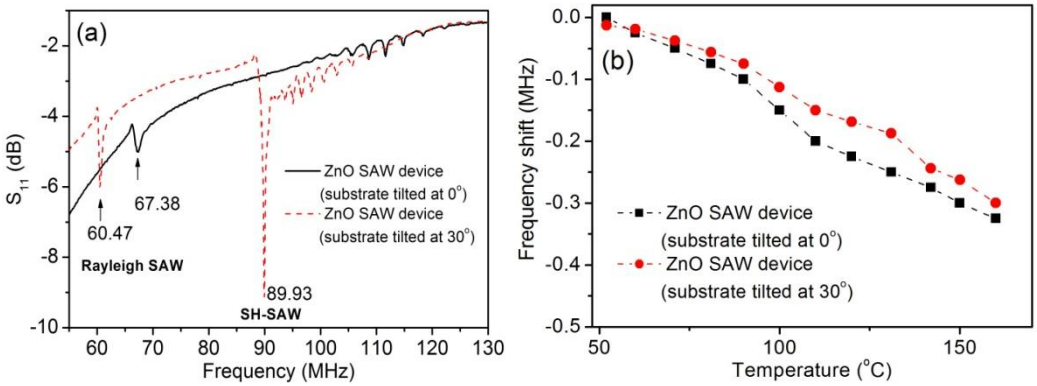

Figure 3.(a) Reflection spectra (S_{11}) of the ZnO SAW devices using the ZnO film grown with different substrate tilting angles; (b) Frequency shifts of the Rayleigh mode with the temperature for the ZnO SAW devices with vertical columnar structure and substrate tilting angle of 30°.

Because the film thickness varies slightly during the growth process on the silicon substrate using the GLAD process, the optical interferences or fringes can be clearly observed on the surface of the inclined ZnO film. Due to the anisotropic effect induced by the inclined angled columnar and crystal structures, it is needed to investigate the differences of the SAW excitation directions on the reflection spectra of the ZnO SAW devices. We selected the device with a spatial period of 64 μm with the substrate tilting angle of 30°, and two pairs of the IDTs with their directions vertical and parallel to the interference fringes, respectively. Figure 4 shows that there is a frequency difference of ~0.41 MHz between the two peaks of Rayleigh waves for the different excitation directions. Whereas the peak shift of SH-SAW is only ~0.04 MHz. There are weak and ripple signals of Sezawa waves, thus it is difficult to identify their frequency differences along different directions.

Comparing the peak shift differences between Rayleigh waves and SH-SAWs, the effect of the excitation direction has been shown as a significant factor on the Rayleigh waves, as opposed to SH-SAW. The main reason is that the longitudinal component of the Rayleigh wave is very sensitive to the film thickness and the changes of the non-centrosymmetric polarization of the wurtzite structure along the

[0001] orientation in ZnO film [40]. Whereas the transverse shear vibrations of SH-SAWs cause the distortion or displacement of SH-SAWs, mostly parallel to the surface of the substrate, and the in-plane acoustic propagation is confined within the film and interface between the inclined ZnO film and substrate [6]. In addition, the frequencies excited from the pair of IDTs with the same directions do not show apparent differences, which means that the slight difference in film thickness does not cause apparent changes within the region of the two IDTs. Therefore, the thickness effect will not cause apparent peak shift for the SH-SAWs. The excitations with orthogonal directions on the inclined film-based SAW device show the anisotropic effect for Rayleigh waves and SH-SAWs.

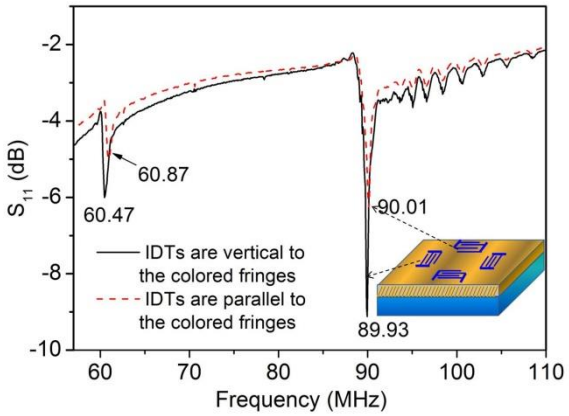

Figure 4. Effects of the excitation directions on the reflection spectra (S_{11}) of the SAW devices fabricated using the ZnO film with a substrate tilting angle of 30°. The inset shows that the excitation directions of IDTs are vertical and parallel to the interference fringes of the inclined ZnO films, respectively.

3.3. Acoustofluidics performance

Figure 5a illustrates that the Rayleigh waves are propagated on the surface of the inclined ZnO film and then dissipated into the liquid droplet. The coupled energy and momentum of the Rayleigh waves were attenuated into liquid along the Rayleigh angle (ϕ_R), which is defined by the Snell law of diffraction:

$\phi_R = \sin^{-1}(V_l/V_s)$, where V_l and V_s are the velocities of the Rayleigh waves in the liquid and ZnO film, respectively [11,15].

Figure 5b shows one captured top-view image of the internal flow (or streaming) pattern of a droplet with a volume of 10 μL on the ZnO SAW device with a substrate tilting angle of 30° at a resonant frequency of 60.47 MHz and a power of 0.1 W, which is similar to the patterns for the Rayleigh SAWs using $LiNbO_3$, ZnO and AlN SAW devices [11,45,46]. A quasi-stable butterfly-like pattern consisting of the double vortexes in the droplet is induced by the ZnO/Si Rayleigh mode SAW as shown in Figure 5b.

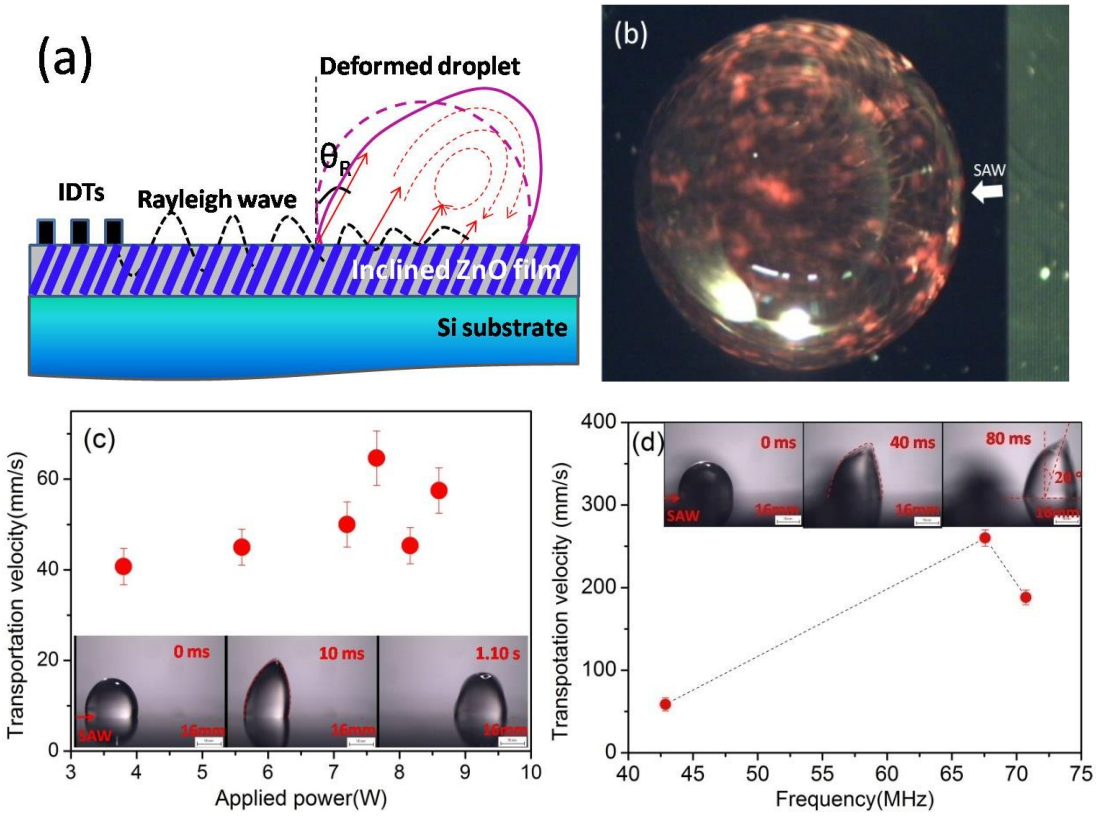

Figure 5. (a) A schematic illustration of cross-section view for the coupling and flow patterns of the SAWs within the liquid droplet; (b) top-view image of the flow pattern of a droplet (10 μL) captured at 60.47 MHz and a power of 0.1 W using the Rayleigh mode of ZnO SAW device with a substrate tilting angle of 30°; (c) the transportation velocity of a 2 μL droplet on the hydrophobic surface of ZnO SAW devices induced by Rayleigh mode that were excited by the IDTs parallel to the thin-film interference fringes; the

inset show the snapshots of the transportation of the droplet driven by Rayleigh SAWs with a applied power of 3.8 W; (d) the transportation of the droplet with a volume of 2 μL on the hydrophobic surface of ZnO SAW devices induced by Rayleigh SAWs that were excited by the IDTs vertical to the fringes at different resonant frequencies, the inset shows the Rayleigh angle of the coupled SAWs with an applied power of 9.1 W at a resonant frequency of 42.87 MHz.

With the increased SAW power, the sessile droplet is deformed with asymmetric contact angles and starts to slide along the propagation direction of the SAW. Figure 5c shows the transportation velocities of the 2 μL droplet on the hydrophobically treated surface of ZnO SAW devices induced by Rayleigh SAWs at different powers applied to the IDTs parallel to the interference fringes. The transportation velocity of the droplet is quite low and varied around ~50 mm·s^{-1}, with the applied power increased from 3.8 W to 8.6 W. Figure 6d shows examples of the captured images for the droplet transportation with a volume of 2 μL on the hydrophobic surface of ZnO SAW devices, where Rayleigh SAWs were excited by the IDTs with a propagation direction vertical to the thin-film interference fringes. The shape of the deformed droplet is significantly elongated along the Rayleigh angle (θ_R) at the resonant frequency. The measured jetting angle of ~20° is very close to the theoretically Rayleigh value of 20.95° [11] as shown in the inset of Figure 5d. The transportation velocity of the droplet on the film surface is determined as 260 mm·s^{-1} for the resonant signal at 67.66 MHz with an applied power of 9.1 W and 188 mm·s^{-1} for the resonant frequency of 70.72 MHz at the same power.

Comparing the values of transportation velocities produced using the IDTs vertical to the fringes with those parallel to the fringes, it is found that the Rayleigh SAWs excited from both directions induce droplet pumping. However, the transportation efficiency of the droplet using IDTs that is vertical to the fringes is

relatively higher than that using IDTs that parallel to the fringes under the same applied power and frequency.

The coupling energy and momentum induced by the interfacial interaction of the viscous liquid with the SH-SAWs is very weak. At a very higher power of tens of watts, large vertical pressure gradient is generated, resulting in very weak random streaming patterns, which has been reported in the literature [42, 47, 48].

3.4. Biosensing using biotin and streptavidin

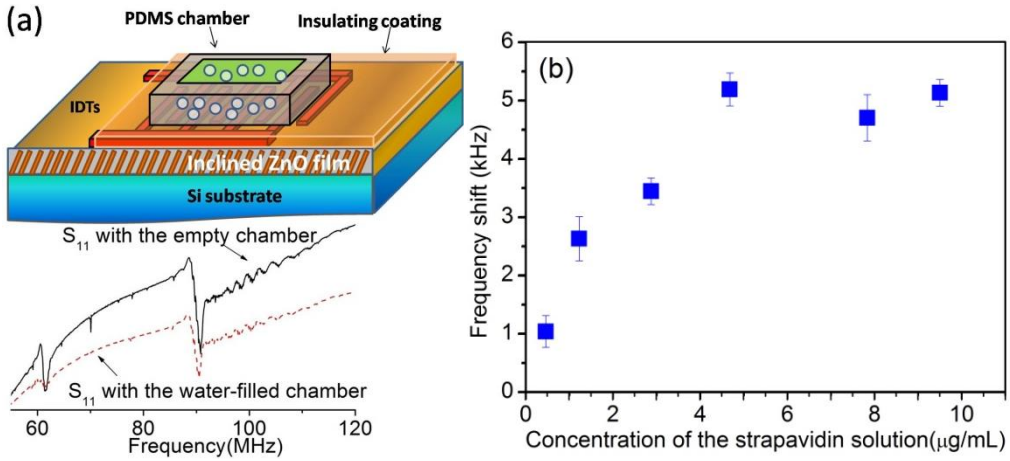

Figure 6. (a) A schematic illustration of the biosensing using the biotin and streptavidin detected by the SH-SAWs and S_{11} of the ZnO SAW device with the empty and water-filled chamber; (b) the frequency shift of the SH-SAWs with the different concentrations of the streptavidin solution.

Figure 6a shows a schematic illustration of the system that comprises a PDMS chamber with the silica-coated IDTs of the ZnO SAW device. Considering the difference of the acoustic properties of the dual mode SAWs in the liquid, the Rayleigh waves nearly disappears after applying the liquid chamber on top of the IDTs. Their reflection signals can be hardly identified from the reflection signals of S_{11} due to the attenuation of the acoustic energy into the liquid, as shown in Figure 6a. Whereas the magnitude of the

signal for SH-SAWs is dampened slightly and the frequency is also slightly decreased to~89.9 MHz, and thus the SH-SAWs can be used for biosensing within the liquid chamber.

Coupling of streptavidin and biotin normally involves four identical subunits of the streptavidin protein binding with four biotin molecules and was widely applied on the surface acoustic wave biosensors with specific immune responses [49-51]. Figure 6b shows the frequency shifts of the biosensor response as a function of the concentration of the streptavidin conjugated microspheres ranging from 0.5 $\mu g \cdot mL^{-1}$ to 9.5 $\mu g \cdot mL^{-1}$. The frequency shift is increased with the increase of the concentration of streptavidin microspheres in the chamber, mainly due to mass loading effect and viscoelasticity changes on the bottom surface of the chamber [49,51]. From Figure 6b, the mass sensitivity is gradually changed around a concentration of 5 $\mu g \cdot mL^{-1}$. For example, it is determined as 930 $Hz \cdot (\mu g \cdot mL^{-1})^{-1}$ when the concentration is less than 3 $\mu g \cdot mL^{-1}$ and becomes 15 $Hz \cdot (\mu g \cdot mL^{-1})^{-1}$ when the concentration is larger than 6 $\mu g \cdot mL^{-1}$. The differences are mainly due to the saturated bio-reaction of the streptavidin with the biotin due to the limited area of the bottom surface of the chamber at a higher concentration of streptavidin.

4. **Conclusion**

In this paper, the inclined ZnO films were successfully deposited using DC magnetron sputtering with a substrate tilting angle of 30°. XRD pole figure analysis revealed that the inclined ZnO film has a crystal inclination angle of 29.0°±0.5°. Based on the results of the SEM and XRD analysis, this deposited inclined crystal film has a mixed orientation of both vertical crystal orientation and the inclined crystal orientation.SH-SAW and Rayleigh SAW have been simultaneously obtained in the SAW devices made on the inclined ZnO films. The effect of the excitation direction on the frequency change has been observed for the Rayleigh waves and the SH-SAWs. The anisotropic effect of the inclined orientation in the ZnO

films plays an important role on the frequency difference of SH-SAWs excited at orthogonal directions. Results of the excitation direction of Rayleigh SAWs on the acoustofluidics showed that the transportation efficiency of the droplet using IDTs vertical to the interference fringes is relatively higher than those using IDTs parallel to the fringes under the same applied power. Differences in the acoustofluidics performance of SH-SAW and Rayleigh SAWs show that the multifunctional operations could be combined and performed in the acoustofluidic system using one ZnO SAW device including streaming and transporting using Rayleigh SAWs and effectively biosensing using SH-SAWs.

Credit authorship contribution statement

H. F. Pang: Conceptualization, Investigation, Visualization, Data curation, Writing-original draft, Funding acquisition. R. Tao: Investigation, Formal analysis, Data curation, Funding acquisition. J. Luo: Investigation, Data curation, Funding acquisition. X. Zhou: Investigation, Data curation, Validation. J. Zhou: Validation, Writing-review & editing, Funding acquisition. G. McHale: Funding acquisition， Validation, Writing-review & editing. J. Reboud: Data curation, validation, Writing-review & editing. H. Torun: Data curation，Validation, Writing-review & editing. D. Gibson: Validation, Writing-review & editing. K. Tao: Data curation, Validation, Writing-review & editing. Y. Q. Fu: Conceptualization, Resources, Methodology, Supervision, Project administration, Funding acquisition.

Declaration of competing interest

There are no conflicts to declare.

Acknowledgements

This work was financially supported by the UK Engineering, and Physical Sciences Research Council (EPSRC) grants EP/P018998/1, EPSRC NetworkPlus in Digitalised Surface Manufacturing EP/S036180/1, and Special Interests Group of Acoustofluidics under the EPSRC-funded UK Fluidic Network (EP/N032861/1). We also appreciate the support from EPSRC Centre for Doctoral Training in Renewable Energy Northeast Universities (ReNU) for funding through grant EP/S023836/1, the National Natural Science Foundation of China (NSFC 11504291, 12074309, 52075162, 61274037, 12104320), International Exchange Grant (IEC/NSFC/201078) through Royal Society and the NSFC, the Key Research Project of Hunan Province (2019GK2111), Innovation Leading Program of New and High-tech Industry of Hunan Province(2020GK2015), the Key Research Project of Guangdong Province (2020B0101040002) and the Natural Science Foundation of Changsha (kq2007026). This work was also financially supported by Key Research and Development Program of Guangdong Province (Grant No. 2020B0101040002), Special Projects in Key Fields of Colleges in Guangdong Province (2020ZDZX2097), Research Project in Fundamental and Application Fields of Guangdong Province (2020A1515110561) and Shenzhen Science & Technology Project (Grant no. JCYJ20180507182106754, JCYJ20180507182439574, RCBS20200714114918249, GJHZ20200073109583010). Experimental supports from Dr. Zhefeng Lei, Prof. Xingang Luan, Dr. Chao Zhao, Dr. Yuanjun Guo and Dr. Pep Canyelles Pericas are acknowledged.

References

[1] L. Lamanna, F. Rizzi, V. R. Bhethanabotla, M. De Vittorio, Biosens. Bioelectron., 163(2020)112164

[2] Y. Wang, X. Tao, R. Tao, J. Zhou, Q. Zhang, D. Chen, H. Jin, S. Dong, J. Xie, Y. Q. Fu, Sens. Actuat., A 306 (2020) 111967

[3] M. J. A. Schuetz, E. M. Kessler, G. Giedke, L. M. K. Vandersypen, M. D. Lukin, J. I. Cirac, Phys. Rev. X, 5(2015) 031031

[4]Z. Zhong, H. Zhu, P. Zhang, J. Morizio, T. J. Huang, K. Chakrabarty, IEEE Trans.Biomed. Circuits Syst., 14(2020) 1065-1078

[5] L. Y. Yeo, J. R. Friend, Annu. Rev. Fluid Mech., 46(2014) 379-406

[6] Y. Q. Fu, J. K. Luo, N. T. Nguyen, A.J. Walton, A.J. Flewitt, X.T. Zu, Y. Li, G. McHale, A. Matthews, E. Iborra, H. Du, W.I. Milne, Prog. Mater Sci., 89(2017) 31-91

[7] C.B. Saw, P.M. Smith, P. Edmonson, C.K. Campbell, IEEE Trans. Ultrason. Ferroelectr. Freq. Control 35(3) (1988)390 – 395

[8] C. Caliendo, F. Laidoudi, Sensors, 20(5) (2020) 1380

[9] R. Friend, L. Y. Yeo, Rev. Modern Phys., 83(2011) 647-704

[10] K. Sreenivas, M. Sayer, D. J. Baar, M. Nishioka, Appl. Phys. Lett., 52(9) (1988) 709-711

[11]H.-F. Pang, Y. Q. Fu, L. Garcia-Gancedo, S. Porro, J. K. Luo, F. Placido, J. I. B. Wilson, A. J. Flewitt, W. I. Milne, X. T. Zu, Microfluid. Nanofluid., 15(2013) 377–386

[12] S. Petroni, G. Tripoli, C. Combi, B. Vigna, M. De Vittorio, M.T. Todaro, G. Epifani,R. Cingolani, A. Passaseo, Superlatt. microst., 36(4-6) (2004)825-831

[13] R. Tao, G. McHale, J. Reboud, J. M. Cooper, H. Torun, J.T. Luo, J. Luo, X. Yang, J. Zhou, P. Canyelles-Pericas, Q. Wu, Y. Fu, Nano Lett., 20(2020) 3263-3270

[14] H. Bachman, Y. Gu, J. Rufo, S. Yang, Z. Tian, P.-H. Huang, L. Yu, T. J. Huang, Lab on a Chip, 20(2020) 1281-1289

[15] Y.Q. Fu, J.K. Luo, X. Du, A.J. Flewitt, Y. Li, A. Walton, W.I. Milne, Sens. Actuat. B., 143(2010) 606-619

[16] F. Martina, M. I.Newton, G. McHale, K. A. Melzak, E. Gizeli, Biosens. Bioelectron., 19(6) (2004) 627-632

[17] T. Kogai, H. Yatsuda, J. Kondoh, IEEE Trans. Ultrason. Ferroelectr. Freq. Control, 4(9) (2017)1375-1381

[18] E. Berkenpas, P. Millard,M. Pereira da Cunha, Biosens. Bioelectron., 21(12) (2006) 2255-2262

[19] K. Takayanagi, J. Kondoh, Japan. J. Appl. Phys., 57(7S1) (2018) 07LD02.

[20] J. Luo, A. Quan, C. Fu, H. Li, J. Alloys Comp., 693(2017)558-564

[21] A. Fardeheb-Mammeri1, M. B. Assouar, O. Elmazria, J.-J. Fundenberger, B. Benyoucef, Semicond. Sci. Technol. 23(2008) 095013

[22] C.-K. Jen, K. Sreenivas, M. Sayer, J. Acoust. Soc Am., 84(1988) 26-29

[23] T. Yanagitani, N. Morisato, S. Takayanagi, M. Matsukawa, Y. Watanabe, IEEE Trans. Ultras. Ferroelectr. Freq. Control, 58(2011) 1062-1068

[24] G.Rughoobur, M.DeMiguel-Ramos, J.-M. Escolano, E. Iborra, A. J. Flewitt, Sci. Reports **7**(2017) 1367

[25]L. Qin, Q. Chen, H. Cheng, Q.-M. Wang, IEEE Trans. Ultras. Ferroelectr. Freq. Control, 57(8) (2010) 1840-1853

[26] T. Yanagitani. N. Morisato, S. Takayanagi, M. Matsukawa, Y. Watanabe, IEEE Trans. Ultrason.Ferroelectr. Freq. Control, 58(5),(2011) 1062–1068

[27] S. Mukherjee, D. Gall,Thin Solid Films, 527(2013) 158-163

[28] T. Yanagitani, K.Arakawa, K. Kano, A. Teshigahara, M. Akiyama, Ultrasonics Symposium. IEEE, 11-14 Oct. 2010, San Diego, CA, USA.

[29] A. Fardeheb-Nammeri, M. B. Assonar, O. Elmazria, J. J. Fundenberger, B. Benyoucef, Semicond. Sci. Technol., 23 (2008) 095013

[30] A. Kochhar, Y. Yamamoto, A. Teshigahara, K. Y. Hashimoto, S. Tanake, M. Esashi, IEEE Trans. Ultrason. Ferroelectr. Freq. Control, 63(2016) 953–960.

[31] S. Bensmaine, L. Le Brizoual, O. Elmazria, J.J. Fundenberger, M. Belmahi, B. Benyoucef, Diam.Relat. Mater., 17 (2008) 1420–1423

[32]H. F. Pang, Y.Q. Fu, R. Hou, K. Kirk, D. Hutson, X.T. Zu, F. Placido,Ultrasonics, 53(2013)1264-1269

[33] Y.-Q. Fu, H.-F. Pang, H. Torun , R. Tao, G. McHale, J. Reboud, K. Tao, J. Zhou, J. Luo, D. Gibson, J. Luo, P. Hu, Lab Chip, 21(2021) 254-271

[34]X. Yuan, H. Zhou, H. Wang, X.-D. Wang, W.Geng, H. Zhan,K.Kisslinger, L. Zhang, M. Xu, Q. Y. Chen, J. Kang, Appl. Surf. Sci., 509 (2020) 144781

[35] P. Pereira-Silva, A. Costa-Barbosa, D. Costa, M. S. Rodrigues,P. Carvalho, J. Borges, F.Vaz, P. Sampaio, Thin Solid Films 687(2019) 137461

[36]G. Carlotti, D. Fioretto, G. Socino. L. Palmieri, A. Petri, E. Verona, IEEE Ultrasonics Symposium, Honolulu, (1990)449-453

[37] S. Mahieu, P. Ghekiere, D. Depla, R. De Gryse, Thin Solid Films 515(2006) 1229–1249

[38] R. N. Tait, T. Smy, M. J. Brett, J. Vac. Sci. Technol. A 10 (1992)1518-1521

[39] A. Barranco, A. Borras, A. R. Gonzalez-Elipe, A. Palmero, Prog. Mater. Sci., 76 (2016)59–153

[40] H. F. Pang, G. A. Zhang, Y. L. Tang, Y. Q. Fu, L. P. Wang, X. T. Zu, F. Placido, Appl. Surf. Sci., 259 (2012) 747-753

[41] A. Fardeheb-Mammeri, M. B. Assouar, O. Elmazria, J.-J. Fundenberger, B. Benyoucef, Semicond. Sci. Technol.,23(2008) 095013

[42] H.-F. Pang, K.-M. Fan, Y.-Q. Fu, F. Placido, J.-Y. Ma, X.-T. Zu, Adv. Mater. Res., 662 (2013) 580-585

[43] Y. Q. Fu, L. Garcia-Gancedo, H. F. Pang, S. Porro, Y. W. Gu, J. K. Luo, X. T. Zu, F. Placido, J. I. B. Wilson, A. J. Flewitt, W. I. Milne, Biomicrofluidics 6 (2012) 024105

[44] R. Tao, S. A. Hasan, H. Z. Wang, J. Zhou, J. T. Luo, G. McHale, D. Gibson, P. Canyelles-Pericas, M. D. Cooke, D. Wood, Y. Liu, Q. Wu, W. P. Ng, T. Franke, Y. Q. Fu, Sci. Rep., 8 (1)(2018) 9052

[45] M. Alghane Y. Q. Fu, B. X. Chen, Y. Li, M. P. Y. Desmulliez, A. J. Walton, J. Appl. Phys. 109 (2011) 114901

[46] J. Zhou, H. F. Pang, L. Garcia-Gancedo, E. Iborra, M. Clement, M. De Miguel-Ramos, H. Jin, J. K. Luo,S. Smith, S. R. Dong, D. M. Wang, Y. Q. Fu, Microfluid. Nanofluid., 18(4) (2015):37-548

[47] D. S. Brodie, Y. Q. Fu, Y. Li, M. Alghane, R. L. Reuben, A. J. Walton, Appl. Phys. Lett., 99 (2011)153704

[48] C. Fu, A. J. Quan, J. T. Luo, H. F. Pang, Y. J. Guo, Q. Wu, W. P. Ng, X. T. Zu, Y. Q. Fu Appl. Phys. Lett., 110(17) (2017)173501

[49] K. Länge, Bastian, E. Rapp, M. Rapp, Anal. Bioanal. Chem., 391(2008)1509–1519

[50] R. Tao, J. Reboud, H. Torun, G. McHale, L. E. Dodd, Q. Wu, K. Tao, X. Yang, J. T. Luo, S. Todryk, Y.Q. Fu, Lab Chip, **20**(2020)1002-1011

[51] C. Wang, C. Wang, D. Jin, Y. Yu, F. Yang, Y. Zhang, Q. Yao, G.-J. Zhang, ACS Sens., 5(2)(2020)362–369